IEEE Access
Multidisciplinary | Rapid Review | Open Access Journal

Received December 20, 2019, accepted February 1, 2020, date of publication February 10, 2020, date of current version February 18, 2020.

Digital Object Identifier 10.1109/ACCESS.2020.2972589

Coding Biological Current Source With Pulsed Ultrasound for Acoustoelectric Brain Imaging: Application to Vivo Rat Brain

YIJIE ZHOU[1], (Student Member, IEEE), XIZI SONG[1], (Member, IEEE), ZHONGPENG WANG[2], (Student Member, IEEE), XUE ZHAO[1], XINRUI CHEN[1], AND DONG MING[1,2], (Senior Member, IEEE)

[1]Academy of Medical Engineering and Translational Medicine, Tianjin University, Tianjin 300072, China
[2]College of Precision Instruments and Optoelectronics Engineering, Tianjin University, Tianjin 300072, China

Corresponding author: Dong Ming (richardming@tju.edu.cn)

This work was supported in part by the National Key Research and Development Program of China under Grant 2017YFB1300302, in part by the National Natural Science Foundation of China under Grant 81630051 and Grant 81801787, and in part by the China Postdoctoral Science Foundation under Grant 2018M640238.

ABSTRACT Conventional noninvasive electroencephalogram (EEG) is limited to poor spatial resolution due to volume conduction effect. To overcome this limitation, the acoustoelectric effect (AE) based acoustoelectric brain imaging (ABI) is proposed for mapping brain electrical activity in a high temporal and spatial resolution. Through phantom and vivo rat brain experiments, this study investigated a biological current source coding mechanism with pulse focused ultrasound (PFU) at pulse repetition frequency (PRF). First, the current source coding mechanism is deduced in theory. Then, with phantom experiment, the coding relationship between AE signal and PRF is investigated in details. With different PRFs, including 100 Hz, 200 Hz, 500 Hz and 1 kHz, amplitude spectrum analysis results indicate that obvious high amplitude response of AE signal appear at each PRF and corresponding harmonic frequencies. And for different current sources of 10 Hz and 30 Hz, the AE signal oscillate at the the same frequency as corresponding PRF. Additionally, for each PRF, the decoded AE signal is of the same frequency and phase with the current source. Finally, coding mechanism is further validated in vivo rat experiment with different PRFs, including 500 Hz, 1 kHz and 2 kHz. The AE signal envelope and decoded AE signal both have significant correlation with low frequency EEG with ultrasound not only in the low frequency band but also in specific frequency. Also, the mean amplitude of delta rhythm respectively calculated from envelope of AE signal and decoded AE signal are obviously higher than the other rhythms which reflects the brain state of anesthesia or lethargy. These theory and experiment results validate that PFU has a coding effect on current source at PRF and demonstrate the feasibility of restoring current source from the coded AE signal which are critical for making ABI a clinical neuroimaging technique.

INDEX TERMS Acoustoelectric effect, biomedical current source, coding mechanism, focused ultrasound, pulse repetition frequency.

I. INTRODUCTION

Neuroimaging is an effective technology to either directly or indirectly image the structure, function, or pharmacology of the nervous system, which is essential to understand human behavior and gauge the severity of a brain injury [1]. As brain activity is distributed over the 3-D space and time with the millimeter and millisecond scales, it is important to noninvasively image brain dynamics and connectomics with high spatial and high temporal resolution [2]. Neuroimaging modalities, like electroencephalography (EEG), magnetoencephalography (MEG), and functional magnetic resonance imaging (fMRI), are all valuable tools for understanding the brain networks. EEG is spontaneous and

The associate editor coordinating the review of this manuscript and approving it for publication was Ran Su.

rhythmic electrical activities, divided into different frequency bands (delta: 1-4 Hz, theta: 4-8 Hz, alpha: 8-12 Hz, beta: 12-30 Hz, etc.) [3]. Noninvasive EEG offers high temporal resolution (milliseconds), which are of capturing brain dynamics response. However, it suffers from limited spatial resolution due to head volume conduction effect [2], [3]. With sufficient spatial resolution, MEG is also affected by head volume conduction effect [2], [4]. Compared to them, fMRI is of high spatial resolution, while suffers from measuring slow intrinsic signals (evolve over seconds) related to blood oxygen saturation or metabolic activity [5]. To overcome the shortcoming of conventional neuroimaging techniques, transcranial focused ultrasound has been adopted for electrophysiological neuroimaging and noninvasive acoustoelectric brain imaging (ABI) has been proposed. Due to the spatial focality and noninvasiveness of focused ultrasound, ABI is a potential neuroimaging technique with high spatiotemporal resolution [6].

According to acoustoelectric (AE) effect [7], current source coding mechanism has been investigated and applied for ABI, which is the basic principle to accomplish spatial selectivity for high resolution electrophysiological neuroimaging. There are some studies focused on acoustoelectric coupling principle based on electrical and acoustic parameters such as current density, current flow direction, acoustic pressure and center frequency. In 2000, B. Lavandier *et al*. proved that it was possible to quantitate the acoustoelectric interaction signal once the ultrasonic vibration potential due to the Debye effect has been subtracted [8]. The acoustoelectric interaction signal was shown to be directly proportional to both the applied acoustic pressure and current. In 2007, R. S. Witte *et al*. injected ionic current into the abdominal segment of the lobster nerve cord and measured ultrasonic spatial coded electrophysiological signal [9]. It indicated that the acoustoelectric signal was directly proportional to focal pressure and current density, and also sensitive to the direction of current flow. Based on these investigated source coding mechanism, R. Olafsson *et al*. proposed ultrasound current source density imaging (UCSDI) with spatial resolution superior to conventional methods in 2008. It is able to accurately locate sources and sinks to within 1 mm of their actual positions [10]. In 2015, Y. Qin *et al*. demonstrated that UCSDI was potentially capable of real-time 3D cardiac activation wave mapping of the live rabbit heart [11]. With the same acoustic pressure, 1-MHz transducer showed better spatial resolution than the 0.5-MHz transducer. Experiments indicated that center frequency takes effect in coding current source. In 2016, B. He presented a concept on acousto-electrophysiological neuroimaging (AENI). Injecting ultrasound energy, the AENI promises to offer a desirable high spatiotemporal resolution neuroimaging capability suitable for human brain mapping with millisecond temporal resolution and millimeter spatial resolution [12]. Further, R. S. Witte *et al*. demonstrated 4D ABI in a novel human head and brain phantom for detecting and imaging electrical current flow patterns [13]. These studies revealed and adopted current source coding mechanism mainly involving the relationship between ultrasonic spatial coded signal and current density, current flow direction, acoustic pressure and center frequency of ultrasound.

Recently, a significant electrophysiological signal was observed at pulse repetition frequency (PRF) only when pulse focused ultrasound (PFU) was applied to living rat brain [14]. In addition, produced by amplitude demodulation of the EEG signal at 1050 Hz, the measurement of gamma band (>30 Hz) brain activity was consistent with direct measurements of that activity without ultrasound. However, to the knowledge of the author, there was no study involving the possible source coding mechanism with PRF of PFU. Utilizing PFU and PRF, what is the specific relationship between AE signal and source? These unclear questions are critical for providing theoretical support for ABI to be a clinical neuroimaging technique.

To further explore the exact coding mechanism with PFU at PRF, phantom and vivo experiments were implemented in this study. The rest of the paper is organized as follows. Section II introduces the principle of ABI and source coding mechanism. Section III describes the experimental process of phantom and vivo rats in details. The results of spectral and rhythm analysis, and decoding are reported in Section IV. More analysis is further discussed and a brief conclusion is drawn in Section V.

II. THEORY

A. ACOUSTOELECTRIC EFFECT

Acoustoelectric effect is the physical foundation of ABI. It refers to conductivity modulation induced by acoustic pressure when ultrasound beam traversing biologic tissue. It is described as [15]

$$\frac{1}{\Delta\sigma} = -\frac{1}{\sigma_0} K \Delta P \tag{1}$$

where σ_0 is the conductivity. And $\Delta\sigma$ is the conductivity change of the tissue due the ultrasonic pressure change ΔP. K is the AE interaction constant. The AE effect shows that tissue conductivity is modulated most at the focal region of the ultrasound beam. The local change in conductivity produces a current modulation when electrical current passes through tissue. According to previous studies, only a very small change in conductivity is induced by a change in pressure (e.g. 0.1% per MPa for NaCl solution) [15].

B. LEAD FIELD AND ACOUSTOELECTRIC SIGNAL

A pair of electrodes is called a lead. The distribution of the sensitivity of the lead is called lead field. Based on the reciprocity theorem, the lead field $\tilde{J}_i^L$ is exactly the same as the current flow field resulting from the application of a unit current, called the reciprocal current, to the lead [16], [17]. The voltage V_i measured by lead i is

$$V_i = \iiint \frac{1}{\sigma_0} \left(\tilde{J}_i^L \cdot J^I \right) dxdydz \tag{2}$$

where $\tilde{J}_i^L = \tilde{J}_i^L(x, y, z)$ is the lead field of lead i and $J^I = J^I(x, y, z)$ is the distributed current source. Integration variables (such as x, y, and z) are omitted from subsequent equations, except when needed for clarity. According to (2), the lead field has an important property: it equals the lead sensitivity distribution. This means that at each point of the volume conductor, the absolute value of the lead field current density equals to the magnitude of the lead sensitivity, and the direction of the lead field current equals the direction of the lead sensitivity.

When ultrasound traversing a tissue, the conductivity distribution is

$$\frac{1}{\sigma} = \frac{1}{\sigma_0} - \frac{1}{\sigma_0} K \Delta P \tag{3}$$

Substituting (3) into (2) leads to

$$V_i = V_i^{LF} + V_i^{AE} \tag{4}$$

$$V_i^{LF} = \iiint \frac{1}{\sigma_0} \left(\tilde{J}_i^L \cdot J^I \right) dxdydz \tag{5}$$

$$V_i^{AE} = \iiint (-\frac{1}{\sigma_0} K \Delta P)(\tilde{J}_i^L \cdot J^I) dxdydz \tag{6}$$

where V_i^{LF} represents the low-frequency (DC-10 kHz) content of V_i while V_i^{AE} represents the high-frequency (MHz) AE signal. According to (6), a volume image proportional to the local current density distribution is generated by scanning the ultrasound beam across the region of interest.

C. ACOUSTOELECTRIC SIGNAL WITH PULSED ULTRASOUND

Based on acoustoelectric effect, the induced AE modulation is detected according to Ohm's law as a voltage across two or more recording electrodes. The AE signal V_i^{AE} recorded by lead i at position (x, y, z) at ultrasound propagation time t is given by (6). Pulse repetition frequency is a critical physical parameter for ultrasound. Taking PRF into consideration, the ultrasound pressure field is

$$\Delta P = \Delta P(f_{PRF}, t) \tag{7}$$

where f_{PRF} is the PRF, t is the time of ultrasound transmission. Substituting (7) into (6), we have the following form

$$V_i^{AE}(x, y, z, f_{PRF}, t) = \iiint (-\frac{1}{\sigma_0} K \Delta P(f_{PRF}, t))(\tilde{J}_i^L \cdot J^I) dxdydz \tag{8}$$

which is the AE signal equation considering the coding mechanism of PRF. A map of ABI is a collection of V_i^{AE} that form a spatial image of a brain electric activity.

III. METHODS

A. EXPERIMENTAL SETUP IN PHANTOM

1) EXPERIMENTAL SETUP

The experimental setup is shown in Fig. 1. To produce a dipole, two platinum electrodes were immersed in 0.9% saline separated by 15 mm in the sample slot at well-controlled current densities. Another platinum electrode was placed in the middle of the two stimulating electrodes (S+ and S-) as recording electrode for detecting the AE signal. A single-element ultrasound transducer (Olympus, A392S, 1 MHz, 60.0 mm focal length) was placed in a water bath and focused on the S+ from the bottom. An ultrasonic pulse/receiver (Olympus models 5077PR, JP) was applied to drive the ultrasound transducer with short negative square pulses tuned to the transducer center frequency. A 3M film (Tegaderm^{TM}, US) was wrapped at the bottom of sample slot to avoid mixing saline and water. An arbitrary function waveform generator (Rigol DG4162, CN) was utilized as a source for the current injection. Arbitrary waveforms had a frequency band similar to a typical EEG signal (< 200 Hz). AE signals and ultrasonic synchronizing pulse were acquired at the same time.

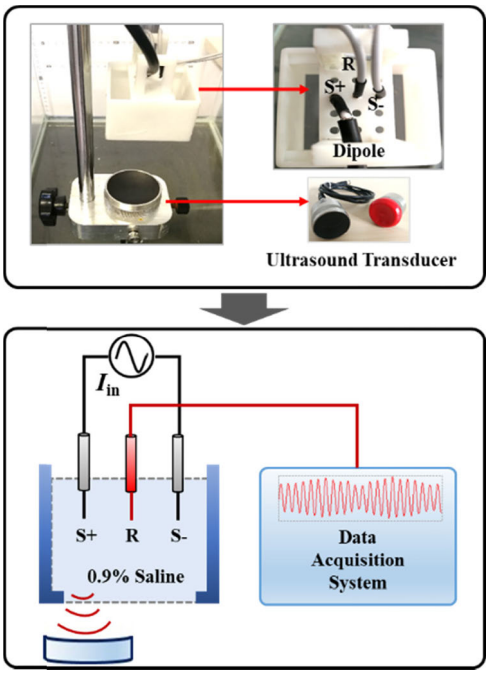

FIGURE 1. Experimental diagram and details in phantom.

TABLE 1. Experimental variables.

Vi	Waveform	A • sin (2πt+φ)
	A	50 mV
	ω	10 Hz, 30 Hz
	φ	0°, 180°
PFU	PRF	100 Hz, 200 Hz, 500 Hz, 1 kHz
	Acoustic Pressure	0.8 MPa
	Transducer Frequency	1 MHz

2) EXPERIMENTAL PARAMETER

As shown in Table 1, all signals were measured under several conditions to investigate modulation effect of AE signal induced by PFU at different PRFs. A sine-wave voltage was applied as source V_i at different frequency (10 Hz and 30 Hz) and phase (0° and 180°). The signals were measured for 60 seconds at different PRFs (100 Hz, 200 Hz, 500 Hz and

1 kHz) of PFU. The transducer frequency was 1 MHz and its acoustic pressure was 0.8 MPa.

Part of phantom experiment has been introduced in our previous work [18]. To further confirm PRF has a coding effect to current source, more detailed phantom experiment is proposed and enlarged to vivo rat brain.

B. EXPERIMENTAL SETUP IN VIVO RATS

1) ANIMALS AND ETHICS STATEMENT

Three adult male Wistar rats (220-260 g) of clean grade were used in this study. Before the experiment, they were housed in standard laboratory cages in the animal house of Tianjin Hospital of Tianjin University, for one week to get acclimated to the research condition (temperature 24 ± 1°C and humidity 50-60% under a 12:12-h light/dark cycle). All experiments were conducted according to the guidelines of the Tianjin Hospital of Tianjin University. Every effort was made to minimize animal suffering and number of animals.

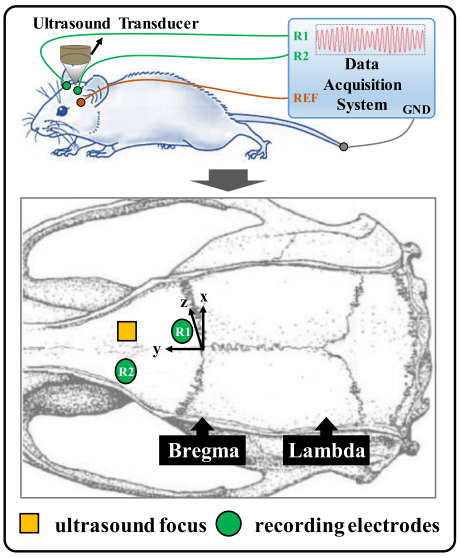

FIGURE 2. Experimental diagram and details in vivo rats.

2) VIVO RAT MODEL

The Wistar rat was chosen for the in vivo study mainly due to its relatively big cranial size and thinner skull among the rat species. Three 12-week-old rat subjects were used, and each was anesthetized using urethane with certain dosage determined by both the rat's weight and the anesthetic duration (5-6 h). Toe and tail pinches were administered to insure adequate depth of anesthesia. The hair over the rat's scalp and caudal regions was carefully removed using an electric hair trimmer to expose the skin. Under anesthesia, two needle platinum recording electrodes (R1 and R2) were implanted into the rats' primary motor cortex referenced to scalp and grounded tail tip (Fig. 2). Define bregma as the origin of a three-dimensional rectangular coordinate system as shown in Fig. 2, the exact location of recording electrodes was (2.00 mm, 0.60 mm, -1.00 mm) for R1 and (-3.40 mm, 0.60 mm, -1.00 mm) for R2.

3) ULTRASOUND PROTOCOL

A single-element ultrasound transducer (1 MHz, 30 mm focal length) was specially customized for smaller volume to fit rat model. It was focused into the rats' primary motor cortex, centered 5 mm below the surface of the skin and into the right hemisphere of the brain, 5 mm away from the closest electrodes. Measured at the full width -3 dB maximum value, the size of focal spot is 20 mm in the axial direction and 2.3 mm (diameter) in the lateral direction. The customized transducer was driven by function waveform generator (Rigol DG1022U, CN), so as to produce a burst of pulses with 10 μs pulse width at PRF of 500 Hz, 1 kHz, and 2 kHz respectively. Measured with the calibrated hydrophone (sensitivity: 0.58 μV/Pa at 1 MHz), the spatial peak temporal average intensity (I_{spta}) is 0.8-3.3 mW/cm^2 in degassed water after transmission through the top of a rat skull. To guide the ultrasound energy onto a certain brain location, a customized conical ultrasound collimator was fabricated. The collimator is of the same length as the focal distance of the transducer. And it was filled with ultrasound coupling gel.

4) EXPERIMENTAL SESSIONS

There were two sessions in this experiment, a sham condition and an experimental group. The sham condition was designed by retaining the ultrasound collimator and turning the transducer away from scalp of the rat without transmitting ultrasound pulses. The endogenous brain activity without ultrasound application was first measured for approximately four minutes. In experimental session, there were three groups at different PRFs (500 Hz, 1 kHz, and 2 kHz) in total. For each group, transcranial pulse focus ultrasound was delivered for 120 seconds without rest.

C. AE SIGNAL MEASUREMENT AND PROCESSING

1) SPECTRUM, ENVELOPE AND DECODING

All signals were acquired, amplified and filtered by SynAmps2 system (Neuroscan, USA). The sampling rate was 20 kHz and band-pass filtering range was 0-3500 Hz. Before signal analysis, the signals were down sampled at 5 kHz. Fast Fourier transform (FFT) was taken to calculate the amplitude spectrum. Then the central frequency of band-pass filter was determined according to spectrum for the next step. To preserve sufficient bandwidth in the decoded signal, the down sampled signal was band-pass filtered around PRF±50 Hz with a 3th order Butterworth filter.

To compute the envelope centered on PRF, absolute value of the narrowband Hilbert transform at PRF was taken [19]. The AE signal is generated by the modulation the electrical field and the acoustic field [20]. Adopting the theory in communication engineering, the PRF was used as the carrier frequency. In order to test the original signal coding at the PRF, a decoding scheme was employed using Matlab's built in *demod* function on the filtered signal [21].

2) FOUR ELECTROPHYSIOLOGICAL SIGNALS

In vivo rats, four kinds of signals were respectively discussed after calculating envelope and decoding. They are low frequency EEG without ultrasound (LF), low frequency EEG with ultrasound (LFU), envelope with ultrasound (EVU) and decoded signal with ultrasound (DCU). These four electrophysiological signals were utilized to study the source coding mechanism with PRF.

3) TIME-FREQUENCY SPECTROGRAM

For more detailed information for time-frequency patterns, the time-frequency spectrogram was adopted to visualize the averaged power changes. Here 2s-data was taken as one trial, then there were 60 trials in total. The averaged power of n trials was calculated according to equation defined as follows [22]:

$$P_{t-f} = \frac{1}{n}\sum_{k=1}^{n}(F_k(f,t)^2) \tag{9}$$

where $F_k(f,t)$ indicates the spectral estimation at frequency f and time t for the kth trial. To determine the difference between EEG of LF and LFU, the averaged time-frequency power (dB) was computed through short-time Fourier transform (STFT) with a 256 points Hanning-tapered window from EEGLAB.

4) CORRELATION ANALYSIS IN FREQUENCY DOMAIN

To investigate the relationships between source and decoded signals, the power spectrum in conditions with ultrasound (i.e. LFU, EVU and DCU) were analyzed by a 2-tailed Pearson correlation test, a widely used statistical test method in EEG parameters [23]. The correlation was normalized with the magnitude of the signals. These tests were made with Matlab's built in correlation function.

IV. RESULTS

A. RESULTS OF EXPERIMENT IN PHANTOM

1) SPECTRAL ANALYSIS OF AE SIGNAL

In order to confirm the frequency component of AE signal, the amplitude spectrum is analyzed by fast Fourier transform. The spectrogram of AE signal with different PRFs (i.e. 100 Hz, 200 Hz, 500 Hz and 1 kHz) is shown in Fig. 3. For each PRF, a high amplitude response of AE signal appears. Besides, obvious amplitude response is also generated at harmonic frequencies of PRF. The results of spectrogram prove that the main frequency component of AE signal coincide with PRF and demonstrate AE signal is relevant to PRF. Based on the spectrum, PRF is adopted as the center frequency of band-pass filter in the following analysis.

2) RELATIONSHIPS BETWEEN SOURCE AND AE SIGNAL

Taking source of 10 Hz as an example, the relationship between source and AE signal are further shown in Fig. 4. For frequency and phase, there is a consistent relationship between envelope of AE signal and source. First,

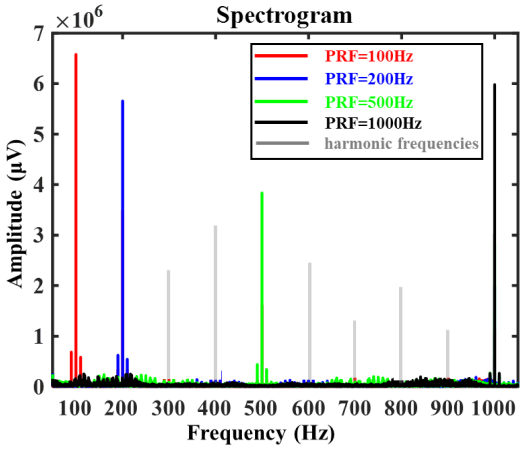

FIGURE 3. Spectrogram of raw AE signal at different PRFs.

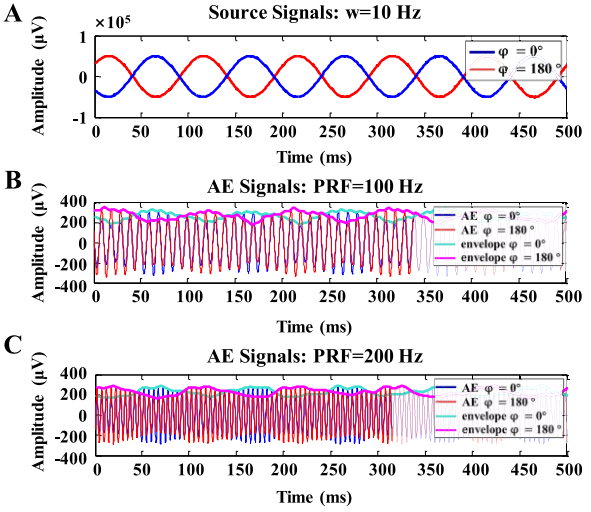

FIGURE 4. Envelope of filtered AE signal at 10 Hz source. (A) shows the source signal of 10 Hz which blue and red curves represent phase of 0° and 180° respectively. (B) and (C) display the corresponding filtered AE signal of the source with the different PRFs (100 Hz and 200 Hz). The envelope of filtered AE signal is plotted in a slightly brighter color (cyanine for phase of 0° and mauve for phase of 180°).

the frequency of envelope is 10 Hz as the same as the source. Besides, the envelope is of the same phase as the source signal. In addition, AE signal which form the envelope oscillate at the same frequency as corresponding PRF. Fig. 4(B) indicates the oscillation frequency of AE signal is 100 Hz as PRF. Fig 4(C) shows the oscillation frequency of AE signal is 200 Hz as PRF as well. As further proof, the frequency of source was set to 30 Hz and the result is in consistent with the above description.

3) DECODING OF AE SIGNAL AT PRF

According to the interaction between source and AE signal, it is highly possible that PRF has a potential coding effect to current source. To restore current source signal, decoding of AE signal is conducted based on coding effect of PRF. Utilizing filtered AE signal as coded signal, Matlab's built

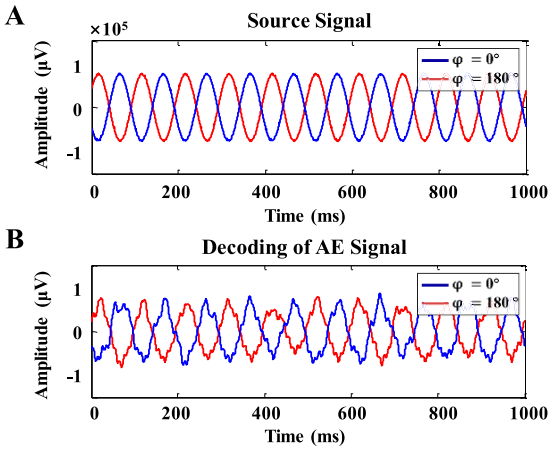

FIGURE 5. Decoding of filtered AE signal at 10 Hz source. (A) shows the source signal of 10 Hz which blue and red curves represent phase of 0° and 180° respectively. (B) shows the decoded AE signal of corresponding source.

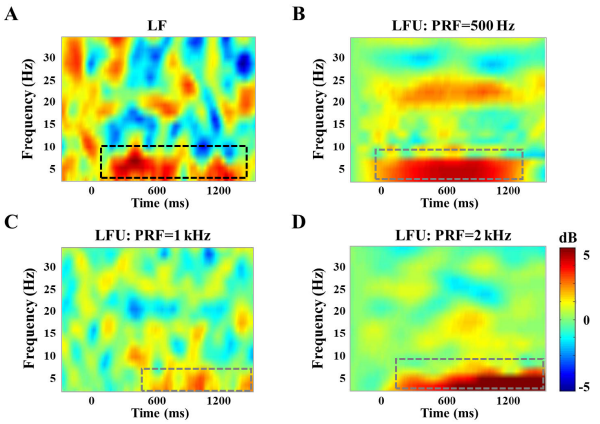

FIGURE 6. Averaged time-frequency maps of LF and LFU. (A) shows the time-frequency map under condition without ultrasound. (B-D) show the time-frequency maps with ultrasound of different PRFs (PRF: 500 Hz, 1 kHz, and 2 kHz). For each map, the *x*-axis shows time in milliseconds, the *y*-axis, frequency in hertz. The color bar indicates power enhancement (red color) or power reduction (blue color).

in *demod* function is employed to implement the decoding algorithm. The PRF of PFU is set as carrier frequency. The source signal of 10 Hz and corresponding decoded signal are presented in Fig. 5 as an example. The blue and red curves represent different source in

phase of 0° and 180° respectively. Comparing Fig. 5(A) and Fig. 5(B), the decoded signal is of the same frequency and phase as the source. Although the decoded signal is not a standard sine wave, the decoding result is meaningful with valuable frequency and phase information.

B. RESULTS OF EXPERIMENT IN VIVO RATS

1) TIME-FREQUENCY SPECTROGRAM OF LF AND LFU

Fig. 6 shows the averaged time-frequency maps across all rats for LF and LFU (PRF: 500 Hz, 1 kHz, and 2 kHz). Under condition without ultrasound as shown in Fig. 6(A), the map of LF presents a clear long-lasting enhancement (marked in black dashed rectangle) of delta (1-4 Hz) and theta (4-8 Hz). In Fig. 6(B-D), the similar feature also can be observed in low frequency EEG with ultrasound of different PRFs as marked in gray dashed rectangle. Specifically, for LFU with PRF of 500 Hz and 2 kHz, the power increases more clearly at the delta and theta frequency band. For LFU with PRF of 1 kHz, there is still a relatively slight enhancement in the map. Therefore, no matter what the PRF is, the long-lasting enhancement of LFU is consistent with those without ultrasound. In other words, it can be considered that ultrasound has little effect on low frequency signals. These results indicate that LFU could be used as the reference of EVU and DCU to study the current source coding mechanism.

2) CORRELATION ANALYSIS IN FREQUENCY DOMAIN

Fig. 7 shows the power spectrum in conditions with ultrasound (i.e. LFU, EVU and DCU). When PRF is 500 Hz, envelope with ultrasound (EVU) has strong correlation with low frequency EEG with ultrasound (LFU) during 8-11 Hz, 15-20 Hz and 27-30 Hz, as well as decoded signal with ultrasound (DCU) and LFU. For PRF of 1 kHz, there is a strong correlation between EVU and LFU during 5-7 Hz, 12-15 Hz and 40-43 Hz, as well as DCU and LFU. With PRF of 2 kHz, a strong correlation can be seen between EVU and LFU during 1-4 Hz, 20-22 Hz and 45-50 Hz, as well as DCU and LFU. According to the correlation analysis in Fig. 7(A), the power spectrum of EVU has a significant correlation with LFU for different PRFs (500 Hz: $r = 0.639$, $p < 0.001$; 1 kHz: $r = 0.667$, $p < 0.001$; 2 kHz: $r = 0.638$, $p < 0.001$). Similarly, as shown in Fig. 7(B), there is a significant correlation between the power spectrum of DCU and LFU for different PRFs (500 Hz: $r = 0.606$, $p < 0.001$; 1 kHz: $r = 0.554$, $p < 0.001$; 2 kHz: $r = 0.487$, $p < 0.001$). Both EVU and DCU have significant correlation with LFU not only in the low frequency band but also in specific frequency. These results further demonstrate the feasibility of current source coding mechanism with PFU at PRF.

3) EEG RHYTHM

Fig. 8 presents the EEG rhythm with different PRFs in all conditions (i.e. LF, LFU, EVU and DCU). Under condition without ultrasound, the amplitude of delta rhythm (37 μV) is higher than others. For LFU, in different PRFs, delta rhythm reaches the highest amplitude (PRF=500 Hz, 35 μV; PRF=1 kHz, 36 μV; PRF=2 kHz, 48 μV). For envelope with ultrasound (EVU), the amplitude of delta rhythm (PRF=500 Hz, 18 μV; PRF=1 kHz, 20 μV; PRF=2 kHz, 18 μV) is also higher than other rhythm. For decoded signal with ultrasound (DCU), the amplitude of delta rhythm (PRF=500 Hz, 13 μV; PRF=2 kHz, 15 μV) is the highest as well. The mean amplitude of delta rhythm is obviously higher than the other rhythms which reflects the brain state of anesthesia or lethargy [24], [25]. These results further confirm that EVU and DCU of the EEG at PRF yielded delta band brain activity is consistent with direct measurements of

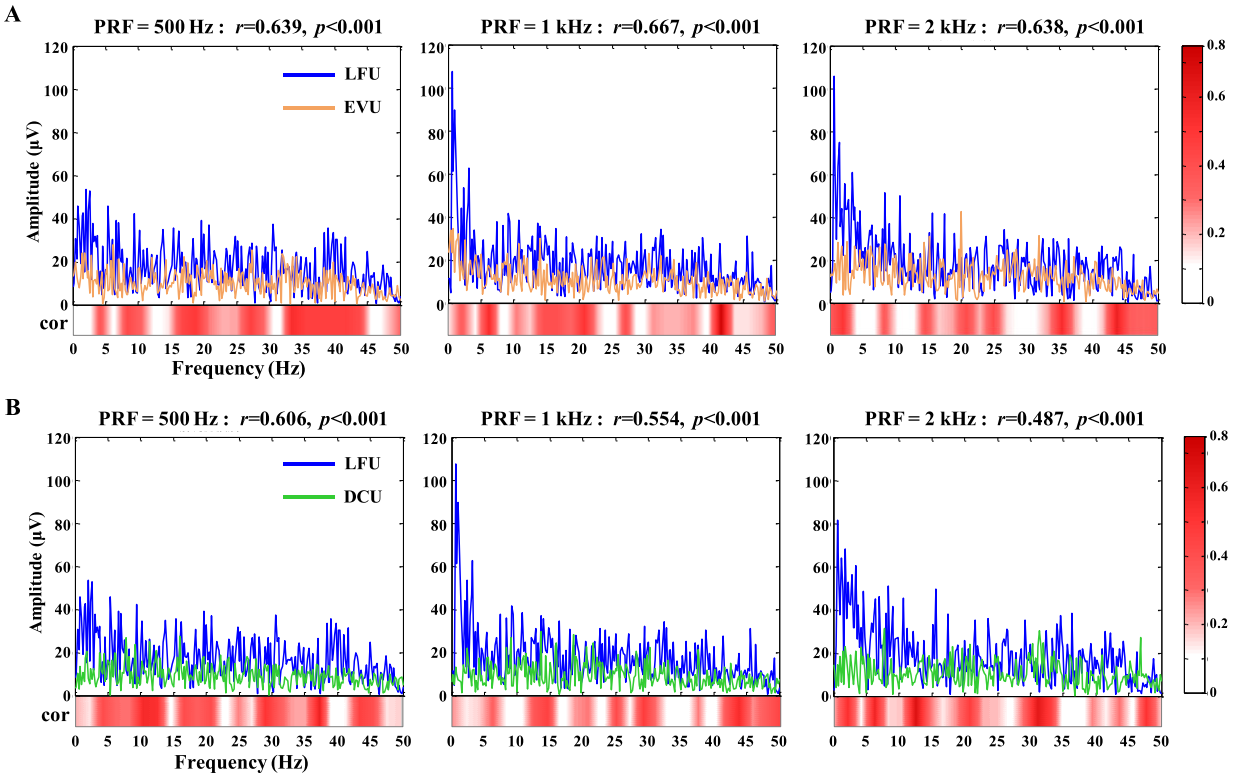

FIGURE 7. Spectrogram and correlation analysis of AE signal with ultrasound. (A) shows the power spectrum of LFU (blue curve) and EVU (orange curve) in in different PRFs. (B) shows the power spectrum of LFU (blue curve) and DCU (green curve) in in different PRFs. Color bar (right): Correlation coefficient reflects the significance of correlation between the different signals. Color map (bottom): The correlation between different signals of corresponding frequency according to color bar. (LFU: low frequency EEG with ultrasound, EVU: envelope with ultrasound, DCU: decoded signal with ultrasound)

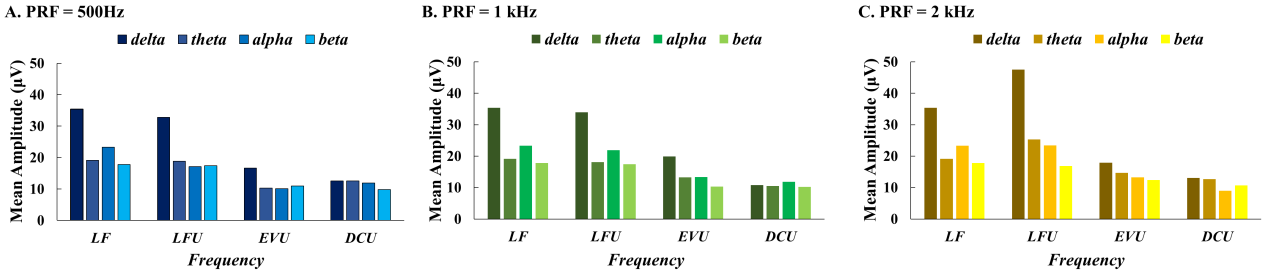

FIGURE 8. EEG rhythm with different PRFs in all conditions, including LF, LFU, EVU and DCU. The mean amplitude of EEG basic rhythm (delta: 1-4 Hz, theta: 4-8 Hz, alpha: 8-12 Hz, beta: 12-30 Hz) is calculated to show the main state of the brain electrical activity. (LF: low frequency EEG without ultrasound, LFU: low frequency EEG with ultrasound, EVU: envelope with ultrasound, DCU: decoded signal with ultrasound).

that activity. Therefore, the proposed current source coding mechanism with PRF might be an available approach towards acoustoelectric brain imaging.

V. CONCLUSION

This study proposes the biological current source coding mechanism with PRF for ABI. First, the source coding mechanism is investigated in theory. Furthermore, the AE signal was detected and analyzed in phantom and vivo rats brain respectively. Experimental results of phantom show that, a high amplitude response of AE signal appears at each PRF. Also, the decoded AE signal is of the same frequency and phase with the current source. In vivo rats experiment, the power spectrum of EVU and DCU has a significant correlation with LFU for different PRFs. For EEG rhythm, EVU and DCU of the EEG at PRF yielded delta band brain activity is consistent with direct measurements of that activity.

In the future, it still deserves further research because the coding and decoding process may be more complicated indeed. In addition, the study of coding mechanism in vivo rats should be expanded to more specific evoked electrophysiological activity to further confirm its feasibility.

In conclusion, PFU has coding effect on current source at PRF which is meaningful for source recovery from coded AE

signal. From the perspective of PRF coding mechanism, this study confirms the feasibility of ABI. Therefore, the proposed source coding mechanism based on PRF of PFU will contribute to the further research and development of ABI and related biomedical imaging techniques.

ACKNOWLEDGMENT

(Yijie Zhou and Xizi Song contributed equally to this work.) The authors would like to thank the ''Tianjin Hospital of Tianjin University'' for providing the opportunity and support to cooperate in this study.

REFERENCES

[1] A. G. Filler, ''The history, development and impact of computed imaging in neurological diagnosis and neurosurgery: CT, MRI, and DTI,'' *Int. J. Neurosurg.*, vol. 7, no. 1, pp. 1–85, Jun. 2009.

[2] B. He, L. Yang, C. Wilke, and H. Yuan, ''Electrophysiological imaging of brain activity and connectivity–challenges and opportunities,'' *IEEE Trans. Biomed. Eng.*, vol. 58, no. 7, pp. 1918–1931, Jul. 2011.

[3] B. He, L. Astolfi, P. A. Valdes-Sosa, D. Marinazzo, S. O. Palva, C.-G. Benar, C. M. Michel, and T. Koenig, ''Electrophysiological brain connectivity: Theory and implementation,'' *IEEE Trans. Biomed. Eng.*, vol. 66, no. 7, pp. 2115–2137, Jul. 2019.

[4] L. Marzetti, Al. Basti, F. Chella, A. D'Andre, J. Syrjälä, and V. Pizzella, ''Brain functional connectivity through phase coupling of neuronal oscillations: A perspective from magnetoencephalography,'' *Frontiers Neurosci.*, vol. 13, p. 964, Sep. 2019.

[5] S. J. Lawrence, E. Formisano, L. Muckli, and F. P. De Lange, ''Laminar fMRI: Applications for cognitive neuroscience,'' *NeuroImage*, vol. 197, pp. 785–791, Aug. 2019.

[6] Y. Qin, P. Ingram, Z. Xu, M. O'Donnell, and R. S. Witte, ''Performance of a transcranial US array designed for 4D acoustoelectric brain imaging in humans,'' in *Proc. IEEE Int. Ultrason. Symp. (IUS)*, Washington, DC, USA, Sep. 2017, pp. 1–4.

[7] J. Jossinet, B. Lavandier, and D. Cathignol, ''The phenomenology of acousto-electric interaction signals in aqueous solutions of electrolytes,'' *Ultrasonics*, vol. 36, nos. 1–5, pp. 607–613, Feb. 1998.

[8] B. Lavandier, J. Jossinet, and D. Cathignol, ''Experimental measurement of the acousto-electric interaction signal in saline solution,'' *Ultrasonics*, vol. 38, no. 9, pp. 929–936, Sep. 2000.

[9] R. Witte, R. Olafsson, S.-W. Huang, and M. O'Donnell, ''Imaging current flow in lobster nerve cord using the acoustoelectric effect,'' *Appl. Phys. Lett.*, vol. 90, no. 16, Apr. 2007, Art. no. 163902.

[10] R. Olafsson, R. S. Witte, S.-W. Huang, and M. O'Donnell, ''Ultrasound current source density imaging,'' *IEEE Trans. Biomed. Eng.*, vol. 55, no. 7, pp. 1840–1848, Jul. 2008.

[11] Y. Qin, Q. Li, P. Ingram, C. Barber, Z. Liu, and R. S. Witte, ''Ultrasound current source density imaging of the cardiac activation wave using a clinical cardiac catheter,'' *IEEE Trans. Biomed. Eng.*, vol. 62, no. 1, pp. 241–247, Jan. 2015.

[12] B. He, ''Focused ultrasound help realize high spatiotemporal brain imaging?-A concept on acousto-electrophysiological neuroimaging,'' *IEEE Trans. Biomed. Eng.*, vol. 63, no. 12, pp. 2654–2656, Dec. 2016.

[13] Y. Qin, P. Ingram, A. Burton, and R. S. Witte, ''4D acoustoelectric imaging of current sources in a human head phantom,'' in *Proc. IEEE Int. Ultrason. Symp.*, Tours, France, Sep. 2016, pp. 1–4.

[14] F. Darvas, E. Mehić, C. J. Caler, J. G. Ojemann, and P. D. Mourad, ''Toward deep brain monitoring with superficial EEG sensors plus neuromodulatory focused ultrasound,'' *Ultrasound Med. Biol.*, vol. 42, no. 8, pp. 1834–1847, Aug. 2016.

[15] B. Lavandier, J. Jossinet, and D. Cathignol, ''Quantitative assessment of ultrasound-induced resistance change in saline solution,'' *Med. Biol. Eng. Comput.*, vol. 38, no. 2, pp. 150–155, Mar. 2000.

[16] S. Finke, R. Gulrajani, and J. Gotman, ''Conventional and reciprocal approaches to the inverse dipole localization problem of electroencephalography,'' *IEEE Trans. Biomed. Eng.*, vol. 50, no. 6, pp. 657–666, Jun. 2003.

[17] J. Malmivuo and R. Plonsey, *Bioelectromagnetism: Principles and Applications of Bioelectric and Biomagnetic Fields*. New York, NY, USA: Oxford Univ. Press, 1995.

[18] Y. Zhou, X. Song, X. Chen, X. Zhao, Y. Ke, and D. Ming, ''A source signal modulation mechanism with pulse focused ultrasound for acousto-electric brain imaging,'' in *Proc. 9th Int. IEEE EMBS Conf. Neural Eng.*, San Francisco, CA, USA, Mar. 2019, pp. 766–769.

[19] F. Darvas, R. Scherer, J. Ojemann, R. Rao, K. Miller, and L. Sorensen, ''High gamma mapping using EEG,'' *NeuroImage*, vol. 49, no. 1, pp. 930–938, Jan. 2010.

[20] R. Yang, X. Li, A. Song, B. He, and R. Yan, ''A 3-D reconstruction solution to current density imaging based on acoustoelectric effect by deconvolution: A simulation study,'' *IEEE Trans. Biomed. Eng.*, vol. 60, no. 5, pp. 1181–1190, May 2013.

[21] S.-S. Yoo, A. Bystritsky, J.-H. Lee, Y. Zhang, K. Fischer, B.-K. Min, N. J. Mcdannold, A. Pascual-Leone, and F. A. Jolesz, ''Focused ultrasound modulates region-specific brain activity,'' *NeuroImage*, vol. 56, no. 3, pp. 1267–1275, Jun. 2011.

[22] W. Yi, S. Qiu, K. Wang, H. Qi, X. Zhao, F. He, P. Zhou, J. Yang, and D. Ming, ''Enhancing performance of a motor imagery based brain–computer interface by incorporating electrical stimulation-induced SSSEP,'' *J. Neural Eng.*, vol. 14, no. 2, Apr. 2017, Art. no. 026002.

[23] F. Wan, J. N. Da Cruz, W. Nan, C. M. Wong, M. I. Vai, and A. Rosa, ''Alpha neurofeedback training improves SSVEP-based BCI performance,'' *J. Neural Eng.*, vol. 13, no. 3, Jun. 2016, Art. no. 036019.

[24] K. Grass, H. Prast, and A. Philippu, ''Ultradian rhythm in the delta and theta frequency bands of the EEG in the posterior hypothalamus of the rat,'' *Neuroscience Lett.*, vol. 191, no. 3, pp. 161–164, May 1995.

[25] J. A. Guidera, N. E. Taylor, J. T. Lee, K. Y. Vlasov, J. Pei, E. P. Stephen, J. P. Mayo, E. N. Brown, and K. Solt, ''Sevoflurane induces coherent slow-delta oscillations in rats,'' *Frontiers Neural Circuits*, vol. 11, p. 36, Jul. 2017.

YIJIE ZHOU (Student Member, IEEE) received the bachelor's degree from the Shandong University of Science and Technology, in 2016. She is currently pursuing the Ph.D. degree in biomedical engineering with Tianjin University. Her major research interests are neural imaging and neural engineering.

XIZI SONG (Member, IEEE) received the Ph.D. degree from Tianjin University, in 2018. She is currently a Lecturer with Tianjin University. Her major research interests include ultrasonic neural functional imaging and ultrasonic neuromodulation.

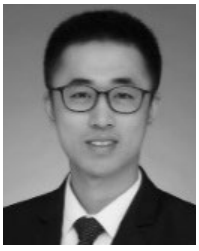

ZHONGPENG WANG (Student Member, IEEE) received the bachelor's degree from the Hebei University of Technology, in 2014. He is currently pursuing the Ph.D. degree in biomedical engineering with Tianjin University. His major research interests are neural rehabilitation and brain–computer interface.

XUE ZHAO received the bachelor's degree from China Agricultural University, in 2018. He is currently pursuing the master's degree in biomedical engineering with Tianjin University. His main research interest is non-invasive deep brain stimulation.

XINRUI CHEN received the bachelor's degree from Jiangsu University, in 2018. She is currently pursuing the master's degree in biomedical engineering with Tianjin University. Her main research interest is fNIRS imaging.

DONG MING (Senior Member, IEEE) received the B.S. and Ph.D. degrees in biomedical engineering from Tianjin University, Tianjin, China, in 1999 and 2004, respectively. He worked as a Research Associate at the Department of Orthopaedics and Traumatology, Li Ka Shing Faculty of Medicine, The University of Hong Kong, from 2002 to 2003, and was a Visiting Scholar with the Division of Mechanical Engineering and Mechatronics, University of Dundee, U.K., from 2005 to 2006. He joined Tianjin University (TJU), as a Faculty at the College of Precision Instruments and Optoelectronics Engineering, in 2006, and has been promoted to a Full Professor of biomedical engineering, since 2011. He is currently a Chair Professor with the Department of Biomedical Engineering, TJU, where he is also the Head of the Neural Engineering and Rehabilitation Laboratory. His major research interests include neural engineering, rehabilitation engineering, sports science, biomedical instrumentation, and signal/image processing, especially in functional electrical stimulation, gait analysis, and brain–computer interface. Furthermore, he has been an International Advisory Board Member of the *The Foot*, and the Editorial Committee Member of *Acta Laser Biology Sinica*, and *International Journal of Biomedical Engineering*, China. He has managed over ten national and international research projects, organized and hosted several international conferences, as the Session Chair or Track Chair over the last ten years and was the General Chair of the 2012 IEEE International Conference on Virtual Environments, Human–Computer Interfaces and Measurement Systems (VECIMS 12). He is the Chair of the IEEE-EMBS Tianjin Chapter.